Journal of Magnetism and Magnetic Materials 576 (2023) 170772

Contents lists available at ScienceDirect

Journal of Magnetism and Magnetic Materials

journal homepage: www.elsevier.com/locate/jmmm

Perfect control of spin, valley and spin-valley-coupled currents in bilayer graphene on WSe_2 magnetic junction: Effect of spin-valley dependent Fermi level and energy gap

Kitakorn Jatiyanon [a], Bumned Soodchomshom [b,*]

[a] Department of Physics, Faculty of Science, Rangsit University, Pathumthani 12000, Thailand
[b] Department of Physics, Faculty of Science, Kasetsart University, Bangkok 10900, Thailand

ARTICLE INFO

Keywords:
Bilayer graphene
WSe_2
Transition metal dichalcogenides
Topological insulator
Spin-valley-transistor

ABSTRACT

We investigate the spin-valley dependent transport properties in a gated bilayer graphene (BG) junction placed on top of WSe2. By means of layer-dependent proximity, the spin–orbit interaction (SOI) is induced in the bottom layer, while the top layer is induced into ferromagnetism by a magnetic insulator. As a result of these differing properties, the Fermi level and energy gap become spin-valley dependent, which could lead to controllable spin- and valley-dependent filtering in the BG system. Our findings predict perfect spin-valley polarization control through gate control, given specific energy and electric field conditions, as well as spin-valley-coupled and spin currents when both the electric-field-induced energy gap and the exchange energy are equal to the SOI strength. We predict that there will be very highly sensitive gate control of −100% to + 100% of spin-valley-coupled polarization for large barrier thickness. Additionally, we predict 100% valley polarization can be controlled by the gate when the exchange energy is equal to the SOI. Furthermore, we found that the performance of the junction to control the polarizations can be enhanced by increasing the thickness of the junction. This work reveals the potential of the BG/WSe2 hybrid structure for spin-valley-current-based electronics, such as spin-, valley-, and spin-valley field-effect transistors.

1. Introduction

Graphene has gained popularity as a cutting-edge material for new devices since its discovery [1–2]. Pristine graphene has the characteristic of being non-magnetic and lacking an energy gap [2]. In monolayer graphene (MG), electrons in the system possess 2-dimensional massless Dirac fermions with two valley degrees of freedom, known as k and k'-valleys. Because of lack of some properties such as gap, magnetism and superconductivity, the doping of graphene with other materials has attracted attention [3–23], as it opens up the possibility of obtaining desired electronic properties. The growth of graphene on substrates such as silicon carbide (SiC) [3,4] and hexagonal boron nitride (hBN) [5] can result in the opening of energy gaps at the Dirac points. Magnetic insulators [6–17] and superconductors [18–21] on top of graphene can be induced into magnetic and superconducting materials, respectively. For instance, the exchange energies of 36 and 80 meV were predicted in MG/EuO [11] and MG/$Y_3Fe_5O_{12}$ [15], respectively. Unlike conventional systems, spin polarization in magnetic graphene has been studied to show the oscillation due to effect of Klein tunneling caused by massless Dirac fermion [22]. When graphene is gapped, Klein tunneling would be suppressed [23]. Valley current may be filtered when applying both vector potential and strain field [24–26]. Specular Andreev reflection and oscillation of Josephson currents are related directly to the massless Dirac fermion nature [18]. Because the planar honeycomb lattice structure formed by carbon atoms results in a weak spin–orbit interaction (SOI) in graphene [2], inducing SOI [27–38] into graphene by external forces is important for application of graphene as a topological material. Graphene with SOI may exhibit topological phases such as quantum spin Hall (QSH), quantum anomalous Hall (QAH) and quantum valley Hall (QVH) phases [39–43]. Recently, the combination of graphene and transition metal dichalcogenides (TMDCs) has become a highly researched topic in the field [28–38], as this proximity effect leads graphene to have SOI. The most fascinating example is the graphene/WSe2 structure, which displays band inversion, leading to novel topological properties [28,30,44,45]. The presence of superconductivity under the topological phase may lead graphene to host Majorana

* Corresponding author.
E-mail addresses: bumned@hotmail.com, fscibns@ku.ac.th (B. Soodchomshom).

https://doi.org/10.1016/j.jmmm.2023.170772
Received 2 March 2023; Received in revised form 8 April 2023; Accepted 22 April 2023
Available online 27 April 2023

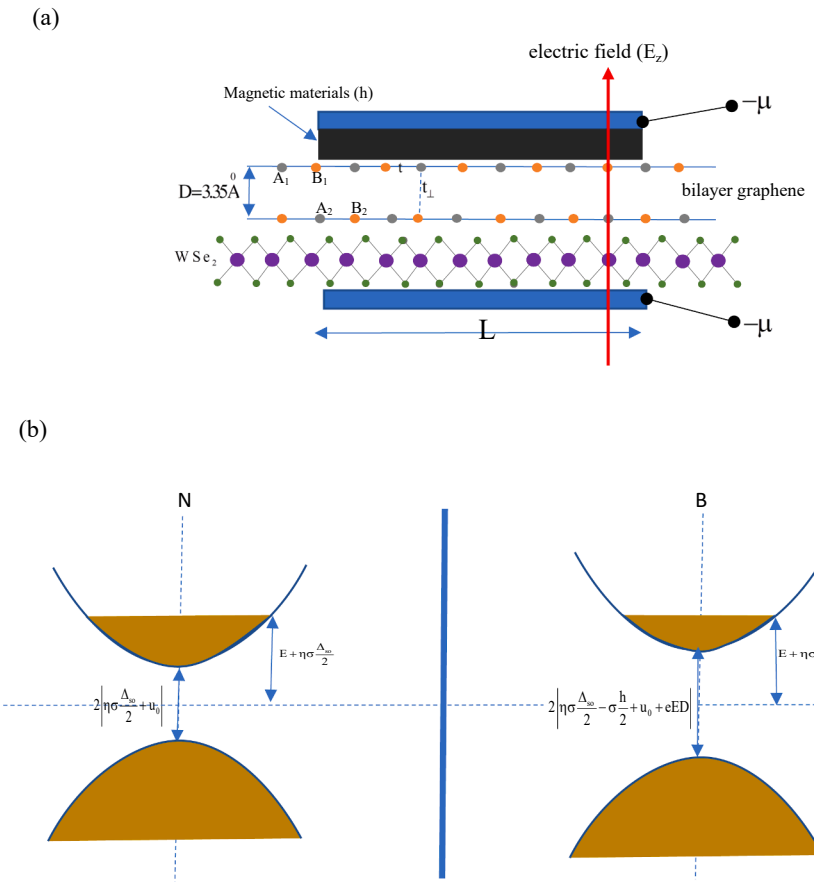

Fig. 1. Illustration of (a) the substrate-induced spin orbit interactionbilayer graphene (BG) based N/B/N junction. BG is placed on top of WSe_2. The exchange field h induced on the top layer with width L is generated by proximity effect using magnetic insulator placed on the top of BG. The perpendicular electric field with magnitude E_z is applied into the barrier region. The gate potential μ is adopted to tune the chemical potential inside the barrier. (b) Illustration of spin-valley dependent band structure and occupied states in normal region (N's) and the barrier (B).

fermion applicable for qubit of topological quantum computation [46]. The experimental study has shown that SOI in graphene on WSe_2 increases by hydrostatic pressure [38]. The spin-split energy dispersion in graphene on WSe_2 have been reported to show the result from proximity effect that leads graphene to have spin polarization and SOI [47].

Recently, proximity effect induced SOI in bilayer graphene (BG) on TMDCs has drawn much attention [32–37,48]. Unlike MG, the energy gap in pristine BG can be tuned easily by perpendicular electric field. Electron in the pristine BG is quadric dispersion [49], instead of linear dispersion like MG. Twisted BG with magic angle exhibits intrinsic unconventional superconductivity [50]. As a specific property, the doping BG with other materials exhibits layer-dependent electronic properties. Since TMDCs are strong interaction with electromagnetic field, graphene/TMDCs is considered as a platform for optospintronics [51–53]. Twisted BG on TMDCs is also applicable for twistronics [37]. Because of displaying band inversion with novel topological properties, BG/WSe_2 systems have a lot of recent investigations [33–36,48]. Layer-dependent proximity effect show intrinsic SOI strength of $\Delta_{so} \sim 2.3$ meV and electric-induced gap of $u_o \sim 5$ meV in encapsulated BG/ WSe_2 structure [35]. The transport in structures that bilayer graphene interfacing with single WSe_2 layer [33–36] and encapsulated by WSe_2 [35,48] are studied. Very recently, optical conductivity in encapsulated BG with WSe_2 has been studied and showed that control of pure-spin valley current and optical switch may be possible [48]. Spin-valley momentum locked state has also predicted [48]. As an effect of layer-dependent proximity, inverted spin-dependent bands by changing the interface layer from the bottom to the top of bilayer graphene [33]. This property is significant for spintronics. Due to the presence of SOI in BG, the structure of BG interfaced with WSe_2 is a topological insulator and rich in spin- and valley- based electronic applications. Proximity-induced ferromagnetism in BG has been one of the interesting topics [34,54–59]. Unlike that in MG, the layer-dependent exchange energy induced in BG leads to more interesting applications. Ferromagnetism induced in one layer of BG have been studied and found that small exchange energies of 1, 3 and 8 meV have been found in BG/Eu [55], BG/ $Cr_2Ge_2Te_6$ [54], BG/ $Cr_2Si_2Te_6$ [56], respectively. The spin-valley dependent electronic transport under the effect of interplay between layer-dependent exchange field and SOI has not been clarified yet. This fundamental property may be basic knowledge for application of spin-valley- based field effect transistors using graphene [33,60,61]. Spin- and valley-tronics are created by the presence of spin and valley currents, which may be found in several low dimensional materials such as silicene, germanene [62–64] and monolayer-TMCDs [65–68]. Although, spin-valley filtering effect have been investigated in many systems, the spin-valley dependent ballistic transport in layer-dependent ferromagnetism in BG on WSe_2 has not yet been reported yet. The new effects that may generate spin-valley filtering in this system is due directly to the layer-dependent ferromagnetism and SOI, which are specific properties of this BG system and different from the previous investigated systems [63,65]. Since bilayer graphene is a potential material for spin-valley based electronics, the theoretical investigation of spin-valley current is important for experimental testing.

In this paper, we would investigate spin-valley ballistic transport properties of bilayer graphene on WSe_2 junction, where WSe_2 are interfaced only with the bottom layer of the BG. In the barrier region with thickness L, the perpendicular electric field and gate potential are applied. The exchange field is also applied only onto the top layer of the BG in the barrier region. The interplay among electric field, SOI and exchange field affected on the spin-valley ballistic transport is focused. This effect resulted from the presence of layer-dependent proximity effect occurs in the BG system, unlike that in the MG system. The spin-valley dependent conductance would be calculated using the Landauer

formula. The spin and valley polarizations are investigated as a function of gate potential. The spin-valley-coupled polarization defined as the combination of the currents carried by electrons with different species from those in the spin and valley currents, discussed in the formalism section. The electronic parameters for the band structure of GB on the WSe_2 substrate are based on ref.[33]. The proximity-induced ferromagnetism only on the top layer in the barrier region may be realized by depositing a magnetic material on the top of BG [54–56]. In this case, the exchange energy 1 meV in the heterostructures BG/Eu [55] and 3 meV in BG/ $Cr_2Ge_2Te_6$ [54] are comparable with the strength of SOI of 1.3 meV induced by MG/WSe_2 structure [33]. The strong spin-valley filtering effect requires the interplay among exchange energy, SOI and electric field.

2. Hamiltonian model

The present model is depicted in Fig. 1a. The current flow in the x-direction. The barrier with thickness L is the gate-control-current region. For our model, the SOI with strength Δ_{so} in the bottom layer and the intrinsic staggered potentials u_o are induced by WSe_2 substrate [33,44]. The perpendicular electric field E_z is applied into the barrier. The exchange energy with strength "h" in the top layer is induced by a magnetic material [54–56]. The gate potential-induced energy μ is applied in the barrier. Therefore, the tight binding Hamiltonian for this BG system may be obtained as [2,44,49]

$$\begin{aligned}\widehat{H} =& -t_0\sum_{<i,j>,n,\alpha}(a^{\dagger}_{n,i\alpha}b_{n,j\alpha}+h.c.)-t_{\perp}\sum_{<i,j>,\alpha}(a^{\dagger}_{1,i\alpha}b_{2,j\alpha}+h.c)\\&+i\frac{\Delta_{so}}{3\sqrt{3}}\sum_{<<i,j>>,\alpha\beta}\nu_{ij}(a^{\dagger}_{2,i\alpha}\sigma^{z}_{\alpha\beta}a_{2,j\beta}+b^{\dagger}_{2,i\alpha}\sigma^{z}_{\alpha\beta}b_{2,j\beta})\\&+\frac{2i}{3\sqrt{3}}\sum_{<i,j>,\alpha\beta}(\lambda_{R1}a^{\dagger}_{1,i\alpha}\left(\vec{\sigma}\times\vec{d}_{ij}\right)_z b_{1,j\beta}+\lambda_{R2}a^{\dagger}_{2,i\alpha}\left(\vec{\sigma}\times\vec{d}_{ij}\right)_z b_{2,j\beta}+h.c.)\\&+u_0\left(\sum_{<i>\alpha}(a^{\dagger}_{1,i\alpha}a_{1,i\alpha}+b^{\dagger}_{1,i\alpha}b_{1,i\alpha})-\sum_{<i>\alpha}(a^{\dagger}_{2,i\alpha}a_{2,i\alpha}+b^{\dagger}_{2,i\alpha}b_{2,i\alpha})\right)\\&+eE_zD\left(\sum_{<i>\alpha}(a^{\dagger}_{1,i\alpha}a_{1,i\alpha}+b^{\dagger}_{1,i\alpha}b_{1,i\alpha})-\sum_{<i>\alpha}(a^{\dagger}_{2,i\alpha}a_{2,i\alpha}+b^{\dagger}_{2,i\alpha}b_{2,i\alpha})\right)\\&-h\sum_{<i>\alpha}(a^{\dagger}_{1,i\alpha}\sigma^{z}_{\alpha\alpha}a_{1,i\alpha}+b^{\dagger}_{1,i\alpha}\sigma^{z}_{\alpha\alpha}b_{1,i\alpha})\quad-\mu\sum_{<i>n,\alpha}(a^{\dagger}_{n,i\alpha}a_{n,i\alpha}+b^{\dagger}_{n,i\alpha}b_{n,i\alpha})\end{aligned}\tag{1}$$

where $a^{\dagger}_{n,i\alpha}(b_{n,j\alpha})$ is creation (annihilation) operator of A(B) sub-lattice at site i(j) with spin polarization α in layer n={1,2}. The notations < i,j > and ≪i,j≫ denote summation overall the nearest and next-nearest neighbor atoms, respectively. The first and second terms represent bilayer graphene Hamiltonian with in-plane hopping energy $t_0 \sim 3.16\,eV$ and the interlayer coupling Hamiltonian for AB-stacking with interlayer hopping energy $t_{\perp} \sim 0.381\,eV$[2,49], respectively. The third term represents in-plane intrinsic SOI only in the bottom layer [44]. This term is standard form of SOI Hamiltonian modeled in several honeycomb latices [39,40,69–72]. $\sigma^{z}_{\alpha\beta}$ is z-axis Pauli matrix element acting on spin space and $\nu_{ij} = 1(-1)$ stands for the next-nearest neighboring hopping being anticlockwise (clockwise). The fourth is the Rashba spin orbit coupling (RSOC) Hamiltonian for the top(bottom) layer with strength $\lambda_{R1(2)}$[44,73]. The fifth term represents the Hamiltonian due to the staggered potential energy u_0 induced by WSe_2 layer. The sixth term represents the Hamiltonian due to the perpendicular electric field "E_z", where $+(-)eE_zD$ is the energy in the top (bottom)layer [2,49]. The seventh term represents the exchange energy "h" in the top layer induced by the magnetic magnetic materials [54–56] (see Fig. 1a). The last term is the gate potential-induced energy $\mu = eV_G$, where V_G is the gate potential.

The single particle 8 × 8 Hamiltonian near the Dirac points from Hamiltonian in Eq. (1) acting on the wave state $\psi = (\varphi_{a1,\uparrow}, \varphi_{a1,\downarrow}, \varphi_{b1,\uparrow}, \varphi_{b1,\downarrow}, \varphi_{a2,\uparrow}, \varphi_{a2,\downarrow}, \varphi_{b2,\uparrow}, \varphi_{b2,\downarrow})$ may be obtained as

$$H_s = \begin{pmatrix} h_1 & \widehat{t}_{\perp} \\ (\widehat{t}_{\perp})^T & h_2 \end{pmatrix}$$

where

$$h_1 = \begin{pmatrix} eE_zD+u_0-h-\mu & 0 & \hbar v_F(\eta p_x-ip_y) & 0 \\ 0 & eE_zD+u_0+h-\mu & 2i\lambda_{R1} & \hbar v_F(\eta p_x-ip_y) \\ \hbar v_F(\eta p_x+ip_y) & -2i\lambda_{R1} & eE_zD+u_0-h-\mu & 0 \\ 0 & \hbar v_F(\eta p_x+ip_y) & 0 & eE_zD+u_0+h-\mu \end{pmatrix}$$

$$h_2 = \begin{pmatrix} \eta\Delta_{s0}-eE_zD-u_0-\mu & 0 & \hbar v_F(\eta p_x-ip_y) & 0 \\ 0 & -\eta\Delta_{s0}-eE_zD-u_0-\mu & 2i\lambda_{R2} & \hbar v_F(\eta p_x-ip_y) \\ \hbar v_F(\eta p_x+ip_y) & -2i\lambda_{R2} & -\eta\Delta_{s0}-eE_zD-u_0-\mu & 0 \\ 0 & \hbar v_F(\eta p_x+ip_y) & 0 & \eta\Delta_{s0}-eE_zD-u_0-\mu \end{pmatrix}$$

and

$$\widehat{t}_{\perp} = \begin{pmatrix} 0 & 0 & 0 & 0 \\ 0 & 0 & 0 & 0 \\ t_{\perp} & 0 & 0 & 0 \\ 0 & t_{\perp} & 0 & 0 \end{pmatrix}\tag{2}$$

The Fermi velocity is $v_F = 3t_0a/2\hbar$ with $a = 2.46\overset{o}{A}$ [2,49]. The notations $\eta = +(-1)$ for $k(k')$ valley and $\sigma = 1(-1)$ for spin $\uparrow(\downarrow)$ are defined. Although, the effect of Rashba spin orbit coupling (RSOC) λ_R in the case of monolayer graphene could be not negligible [44], in bilayer graphene, they may be neglectable in the low energy limit [73]. Recently, it has been shown that when energy E is very small in comparison with the interlayer coupling, $E \ll t_{\perp}$, the effect of RSOC is very weak and may be cancelled, especially in the case of RSOC for the two layers being opposite [73]. Because of this, the model of the Hamiltonian in Eq. (2) may be approximated by setting $\lambda_{R1} = \lambda_{R2} \to 0$, to get the 4 × 4 Hamiltonian acting on $\psi = (\varphi_{a1,\sigma}, \varphi_{b1,\sigma}, \varphi_{a2,\sigma}, \varphi_{b2,\sigma})$ as of the form

$$H = \begin{pmatrix} eE_zD+u_0-\sigma h-\mu & \hbar v_F(\eta p_x-ip_y) & 0 & 0 \\ \hbar v_F(\eta p_x+ip_y) & eE_zD+u_0-\sigma h-\mu & t_{\perp} & 0 \\ 0 & t_{\perp} & \eta\sigma\Delta_{so}-eE_zD-u_0-\mu & \hbar v_F(\eta p_x-ip_y) \\ 0 & 0 & \hbar v_F(\eta p_x+ip_y) & -\eta\sigma\Delta_{so}-eE_zD-u_0-\mu \end{pmatrix}\tag{3}$$

The four-energy band Hamiltonian in eq.3 yields conduction and valence bands for large energy $|E| \geqslant t_{\perp} \sim 0.38eV$[49]. When we consider the low energy regime to investigate the transport property using $E \cong \Delta_{so} \ll t_{\perp}$, the lowest and highest energy bands in 4×4 Hamiltonian are not required. At low energy near the $k(k')$ point, it can be reduced into two components $\psi = (\varphi_{a1}, \varphi_{b2})^T$, since φ_{b1} and φ_{a2} are dimmer states when $|E| \ll t_{\perp}$. The Hamiltonian is thus given as of the 2×2 matrix form

$$H_L = \begin{pmatrix} \eta\sigma\Delta_{so}+u_0+eE_zD-\sigma h-\mu & -\frac{\hbar^2}{2m}(\eta p_x-ip_y)^2 \\ -\frac{\hbar^2}{2m}(\eta p_x+ip_y)^2 & -\eta\sigma\Delta_{so}-u_0-eE_zD-\sigma h-\mu \end{pmatrix}\tag{4}$$

where $m = t_{\perp}/2v_F^2$[2]. Eq. (4) can be rewritten as of the new form to show the spin-valley dependent energy gap and the Fermi energy, as given by [49]

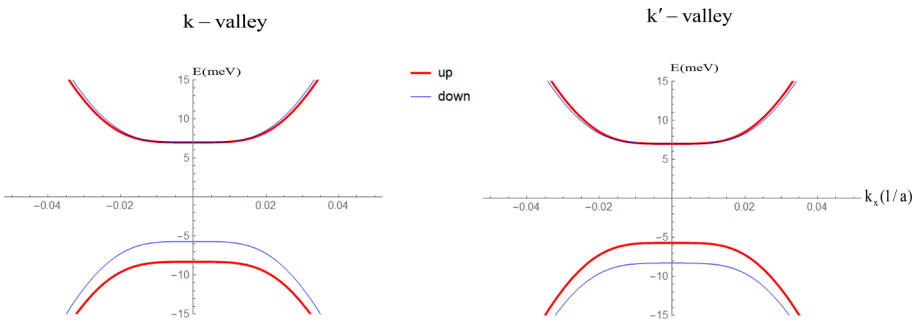

Fig. 2. Shows spin and valley dependent band structure of bilayer graphene on wse$_2$ in normal region. By setting $\Delta_{so} = 1.3meV$ and $u_o = 7meV$ in our model may describe the band structure given in [33].

$$H_L = \begin{pmatrix} \Delta_{\eta\sigma} + u_{\eta\sigma} & -\frac{\hbar^2}{2m}(\eta p_x - ip_y)^2 \\ -\frac{\hbar^2}{2m}(\eta p_x + ip_y)^2 & -\Delta_{\eta\sigma} + u_{\eta\sigma} \end{pmatrix} \tag{5}$$

where $\Delta_{\eta\sigma} = (\frac{\eta\sigma\Delta_{so}}{2} - \frac{\sigma h}{2} + u_0 + eE_zD)$ and $u_{\eta\sigma} = -(\frac{\eta\sigma\Delta_{so}}{2} + \frac{\sigma h}{2}) - \mu$. The Eigen energy is given as

$$E = \pm\sqrt{\left(\frac{\hbar^2}{2m}\right)^2 (p)^4 + (\Delta_{\eta\sigma})^2} + u_{\eta\sigma} \tag{6}$$

where p is the wave vector. As has been seen in Eqs. (5)–(6), the energy gap $E_{gap} = 2\Delta_{\eta\sigma}$ and the Fermi energy $E_F = u_{\eta\sigma}$ are spin-valley dependent. The spin-valley band structure in normal (N) and barrier (B)regions are illustration in Fig. 2a. The occupied states in the N regions are found below $E + \frac{\eta\sigma\Delta_{so}}{2}$, while in the B region are found below $E + (\frac{\eta\sigma\Delta_{so}}{2} + \frac{\sigma h}{2}) + \mu$. Here "E" is the energy $E = eV_{bias}$ due to biased potential V_{bias} of the field effect transistor (FET) crossing source-drain. This special property, **spin-valley dependent gap and Fermi energy in the barrier**, is the main focus in the investigation of transport property that is controlled by the gate at the barrier. This property would play the important role of creating gate control of perfect spin, valley and layer polarizations.

In the normal region, $x < 0$ and $L < x$, we have $h = E_Z = \mu = 0$, to get the Eigen energy from Eq. (6) as of the form

$$E_N = \pm\sqrt{\left(\frac{\hbar^2}{2m}\right)^2 (p)^4 + \left(\frac{\eta s\Delta_{so}}{2} + u_0\right)^2} - \frac{\eta\sigma\Delta_{so}}{2} \tag{7}$$

This formula can describe the band structure of bilayer graphene on WSe_2 given by [33], when we set $\Delta_{so} = 1.3meV$ and $u_o = 7meV$(see Fig. 2). Therefore, our work will study the ballistic transport using these fitting parameters throughout the numerical investigation.

3. Scattering process and transport formulae

In this section, the scattering of electron in the system is studied in BG on WSe_2 system-based N/B/N junction, where in the normal regions (N) $h = E_Z = \mu = 0$, while in the barrier region(B) exchange energy h, electric field E_Z and the gate potential μ are applied (see Fig. 1a). The current is assumed to flow in the x-direction. The barrier is confined in the $0 < x < L$. From Hamiltonian in Eq. (5), the wave function with the incident angle θ and the parallel component $k_P = \sqrt{2m\sqrt{(E - u_{\eta\sigma_N})^2 - \Delta^2_{\eta\sigma_N}}}\sin(\theta)/\hbar$[2,72], defined in the left-N and the right-N, are respectively given as

$$\psi_N(x < 0) = \left[\begin{pmatrix} 1 \\ \alpha_+ \end{pmatrix} e^{ik_{Nx}} + r\begin{pmatrix} 1 \\ \alpha_- \end{pmatrix} e^{-ik_{Nx}} + r'\begin{pmatrix} 1 \\ \beta_- \end{pmatrix} e^{q_{Nx}}\right] e^{ik_P y}$$

and

$$\psi_N(x > L) = \left[t\begin{pmatrix} 1 \\ \alpha_+ \end{pmatrix} e^{ik_{Nx}} + t'\begin{pmatrix} 1 \\ \beta_+ \end{pmatrix} e^{-q_{Nx}}\right] e^{ik_P y}$$

where $\alpha_\pm = \frac{-\hbar^2}{2m}\frac{(\eta k_N \pm ik_p)^2}{(E - u_{\eta\sigma,N} + \Delta_{\eta\sigma,N})} = -\sqrt{\frac{(E-u_{\eta\sigma,N})-\Delta_{\eta\sigma,N}}{(E-u_{\eta\sigma,N})+\Delta_{\eta\sigma,N}}}e^{\pm 2i\eta\theta}, \beta_\pm = \frac{\hbar^2}{2m}\frac{(\eta q_N \pm k_p)^2}{(E - u_{\eta\sigma,N} + \Delta_{\eta\sigma,N})}$

with

$$k_N = \sqrt{(2m/\hbar^2)\sqrt{(E - u_{\eta\sigma,N})^2 - \Delta^2_{\eta\sigma,N}} - k_P^2}\, q_N$$
$$= \sqrt{(2m/\hbar^2)\sqrt{(E - u_{\eta\sigma_N})^2 - \Delta^2_{\eta\sigma_N}} + k_P^2}$$

$$\Delta_{\eta\sigma,N} = \frac{\eta\sigma\Delta_{SO}}{2} + u_0 \text{ and } u_{\eta\sigma,N} = -\frac{\eta\sigma\Delta_{SO}}{2} \tag{8}$$

The wave function in the barrier region is defined as

$$\psi_B(0 \leqslant x \leqslant L) = \left[a\begin{pmatrix} 1 \\ \gamma_+ \end{pmatrix} e^{ik_{Bx}} + b\begin{pmatrix} 1 \\ \gamma_- \end{pmatrix} e^{-ik_{Bx}} + c\begin{pmatrix} 1 \\ \kappa_- \end{pmatrix} e^{q_{Bx}} + d\begin{pmatrix} 1 \\ \kappa_+ \end{pmatrix} e^{-q_{Bx}}\right] e^{ik_P y}$$

where $\gamma_\pm = \frac{-\hbar^2}{2m}\frac{(\eta k_B \pm ik_p)^2}{(E - u_{\eta\sigma,B} + \Delta_{\eta\sigma,B})} = -\sqrt{\frac{(E-u_{\eta\sigma,B})-\Delta_{\eta\sigma,B}}{(E-u_{\eta\sigma,B})+\Delta_{\eta\sigma,B}}}e^{\pm 2i\eta\phi}, \kappa_\pm = \frac{\hbar^2}{2m}\frac{(\eta q_B \pm k_p)^2}{(E - u_{\eta\sigma,B} + \Delta_{\eta\sigma,B})}$

with $k_B = \sqrt{(2m/\hbar^2)\sqrt{(E - u_{\eta\sigma,B})^2 - \Delta^2_{\eta\sigma,B}} - k_P^2}, q_B = \sqrt{(2m/\hbar^2)\sqrt{(E - u_{\eta\sigma,B})^2 - \Delta^2_{\eta\sigma,B}} + k_P^2}$

$$\phi = \sin^{-1}\left(\frac{k_P}{k_B}\right),\ \Delta_{\eta\sigma,N} = \frac{\eta\sigma\Delta_{SO}}{2} - \frac{\sigma h}{2} + u_0 + eE_zD \text{ and } u_{\eta\sigma,B}$$
$$= -\left(\frac{\eta\sigma\Delta_{SO}}{2} + \frac{\sigma h}{2}\right) - \mu \tag{9}$$

The coefficients r and t and are reflective and trans missive coefficients, respectively. r' and t' are decaying states. a,b,c and d are the coefficient of the wave function inside the barrier. They can be determined by matching the wave functions in Eqs. (8) and (9) with the boundary conditions at x = 0 and x = L, respectively given as [2,72]

$$\psi_N(0^-) = \psi_N(0^+)\partial_x\psi_N(0^-) = \partial_x\psi_N(0^+)$$

$$\text{and } \psi_N(L^-) = \psi_N(L^+),\ \partial_x\psi_N(L^-) = \partial_x\psi_N(L^+) \tag{10}$$

4. Transport formulae

The transmission of the junction may be determined by the formula given as

$$T_{\eta\sigma}(\theta) = J_t/J_{in} = (t_{\eta\sigma})^* t_{\eta\sigma} \tag{11}$$

where $J_{t(in)}$ are calculated via the current density of the bilayer graphene

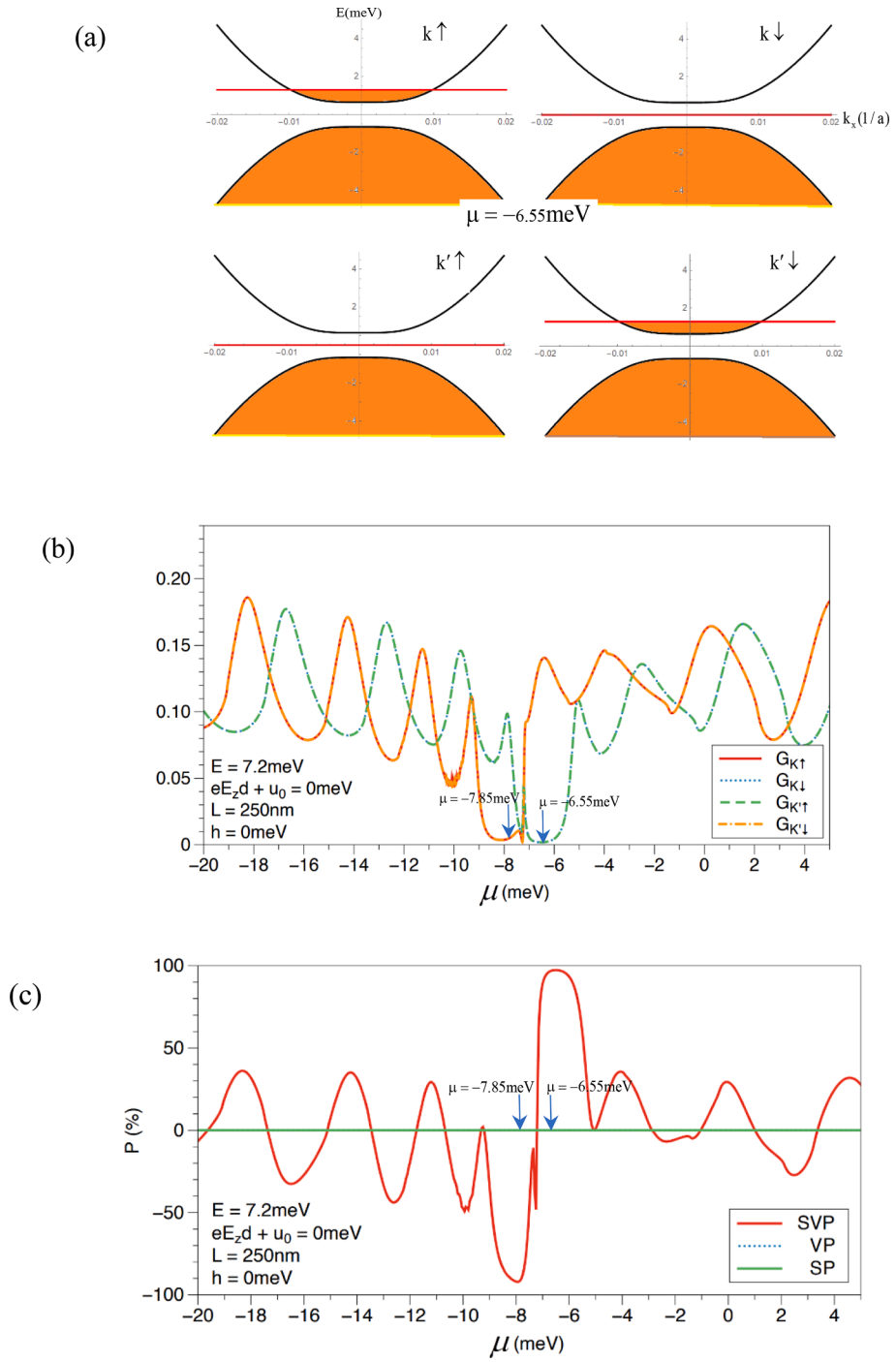

Fig. 3. Shows (a) spin-valley dependent bands and occupied states at $\mu = -6.55meV$. (b) plot of spin-valley dependent conductance as a function of gate potential and (b) the SVP, VP and SP as a function of gate potential for $E = 7.2meV$, $u_0 + eE_zD = 0$, $L = 250nm$ and zero exchange field h = 0. In this case, it is found that VP = SP = 0, while SVP can be controlled from almost −100% to + 100% by varying small value of the gate potential.

system which is determined via the continuity condition [2,72]

$$J_{t(in)} = (i\hbar/2m)\left(\psi^*_{t(in)}\tau_x\partial_x\psi_{t(in)} - \partial_x\psi^*_{t(in)}\tau_x\psi_{t(in)} + 2\psi^*_{t(in)}\tau_y\partial_y\psi_{t(in)}\right) \quad (12)$$

where $\tau_{x,y,z}$ are Pauli spin matrices acting on pseudo spin space and the wave functions $\psi_t = t(1 \quad \alpha_+)^T e^{ik_N x}$ and $\psi_{in} = (1 \quad \alpha_+)^T e^{ik_N x}$ are the transmitted and injected wave states in Eq. (8). Based on the standard Landauer's formalism [74], the dimensionless spin-valley conductance may be thus given as

$$G_{\eta\sigma} = \frac{1}{4}\int_0^{\pi/2} T_{\eta\sigma}(\theta)\cos\theta d\theta \quad (13)$$

Spin and valley polarizations may be respectively defined as

$$SP = \frac{(G_{k\uparrow} + G_{k'\uparrow}) - (G_{k\downarrow} + G_{k'\downarrow})}{G} \times 100\%$$

$$\text{and} \quad VP = \frac{(G_{k\uparrow} + G_{k\downarrow}) - (G_{k'\uparrow} + G_{k'\downarrow})}{G} \times 100\% \quad (14)$$

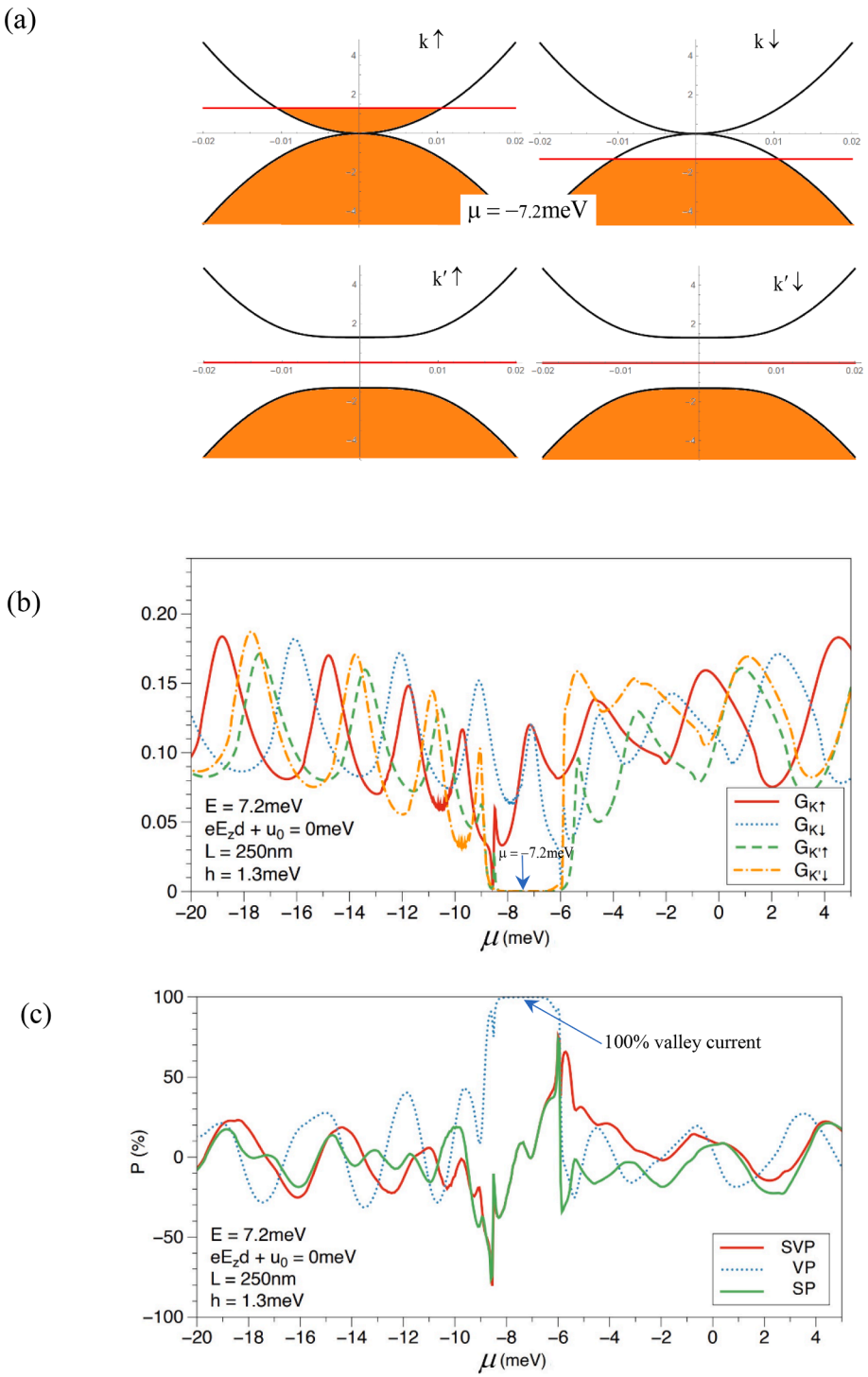

Fig. 4. Shows (a) spin-valley dependent bands and occupied states at $\mu = -7.2meV$. (b) plot of spin-valley dependent conductance as a function of gate potential and (b) the SVP, VP and SP as a function of gate potential for $E = 7.2meV$, $u_0 + eE_zD = 0$, $L = 250nm$ and $h = 1.3meV$. Pure valley current and switching of SVP and SP by varying the gate potential are predicted.

where $G = G_{k\uparrow} + G_{k\downarrow} + G_{k'\uparrow} + G_{k'\downarrow}$ is the total conductance. Since we consider the current governed by the combination of spin and valley, the spin-valley-coupled polarization may be defined as

$$SVP = \frac{(G_{k\uparrow} + G_{k'\downarrow}) - (G_{k\downarrow} + G_{k'\uparrow})}{G} \times 100\% \tag{15}$$

The spin-valley-coupled polarization is to show the imbalance between the spin-valley coupled currents $k\uparrow, k'\downarrow$ and $k\downarrow, k'\uparrow$ .This is the alternating parameter because of the presence of spin and valley currents in graphene. Not only are spin and valley currents applicable but also spin-valley-coupled current.

5. Result and discussions

In the numerical result, the interacting electronic parameters for bilayer graphene grown on WSe_2 are for SOI strength $\Delta_{so} = 1.3meV$ and breaking sublattice gap $u_o = 7meV$, which may be in agreement with fitting curves of the band structure given by ref.[33]. The ballistic

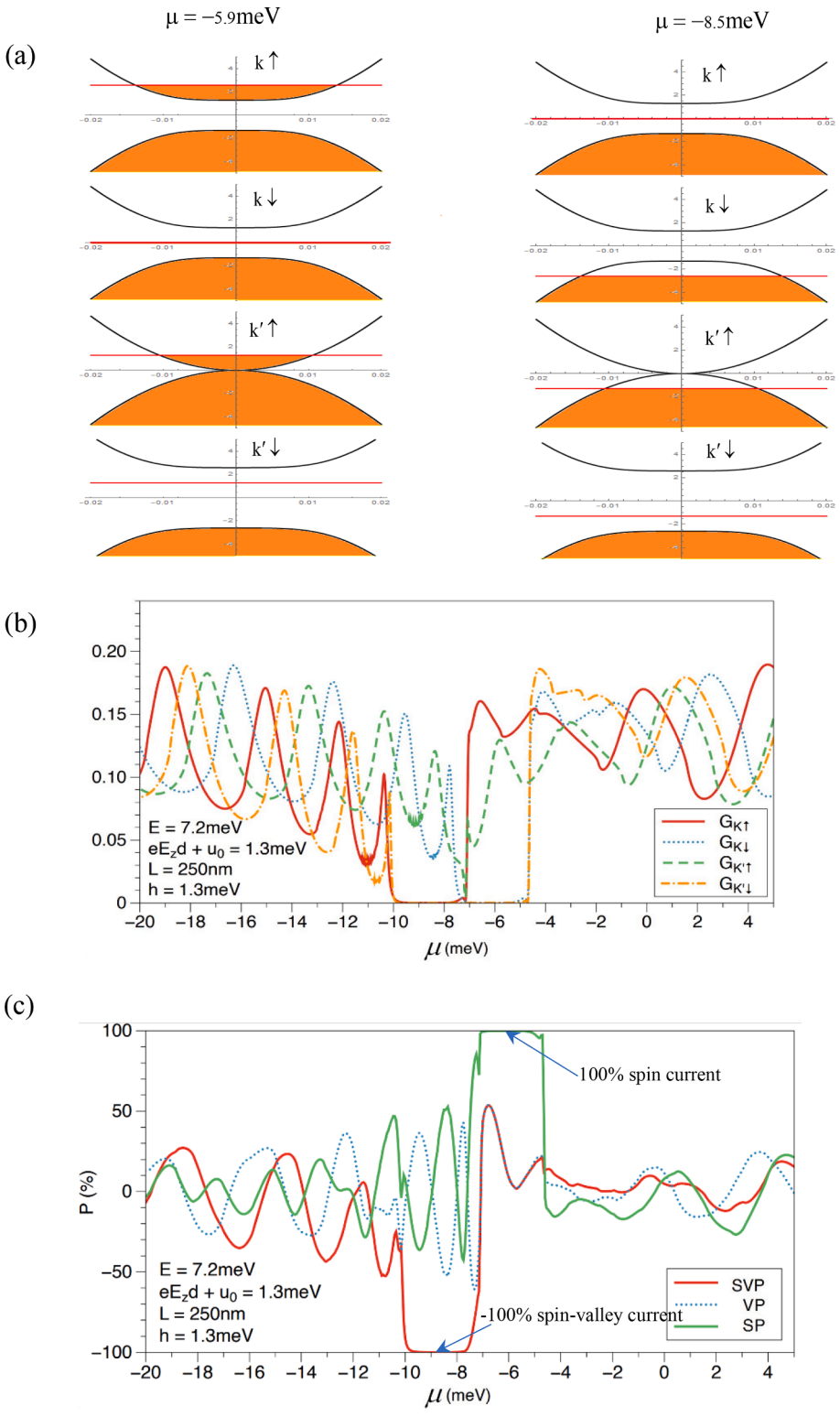

Fig. 5. Shows (a) spin-valley dependent bands and occupied states at $\mu = -7.2meV$. (b) plot of spin-valley dependent conductance as a function of gate potential and (b) the SVP, VP and SP as a function of gate potential for $E = 7.2meV$, $u_0 + eE_zD = 1.3meV$, $L = 250nm$ and $h = 1.3meV$. Pure spin-valley-coupled and pure spin currents are predicted inside the gaps.

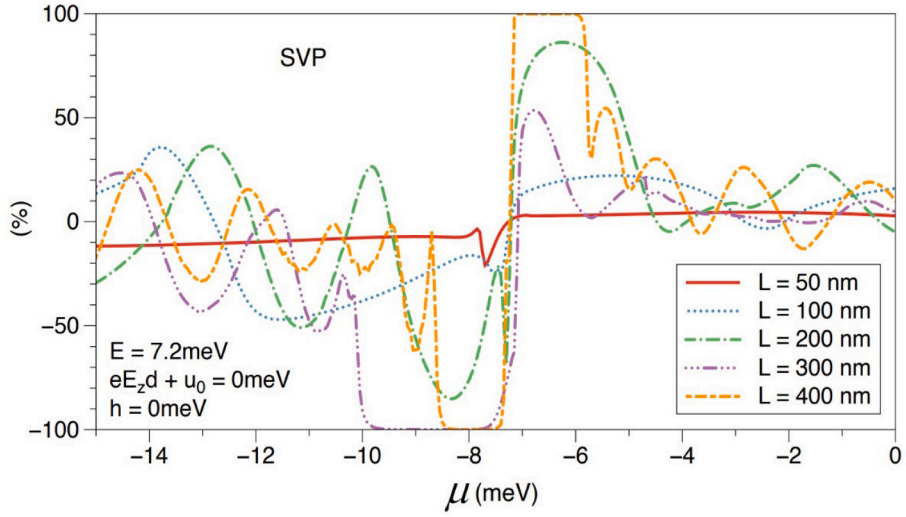

Fig. 6. Study of spin-valley-coupled polarization as a function of gate potential when varying the barrier thickness. changing of svp from−100% to + 100% sharply by varying very small gate potential is predicted for large L.

transport is focused in the case of $E = 7.2meV \cong u_o$. In this case, the system exhibits pseudo-ferromagnet [75], which is considered from the expectation value of the direction of pseudo-spin in normal regions, calculated from

$$\langle \vec{\tau} \rangle = \langle \psi_N | \vec{\tau} | \psi_N \rangle = -\sqrt{1 - \frac{\left(u_0 + \frac{\eta\sigma\Delta_{SO}}{2}\right)}{\left(E + \frac{\eta\sigma\Delta_{SO}}{2}\right)}}(\cos 2\theta \hat{i} + \eta \sin 2\theta \hat{j}) + \frac{\left(u_0 + \frac{\eta\sigma\Delta_{SO}}{2}\right)}{\left(E + \frac{\eta\sigma\Delta_{SO}}{2}\right)}\hat{k}$$

where

$$\psi_N = \frac{1}{\sqrt{2}} \begin{pmatrix} e^{-i\eta\theta}\nu_+ \\ -e^{i\eta\theta}\nu_- \end{pmatrix} \tag{16}$$

is the normalized spinor wave in the N region's with $\nu_\pm = \sqrt{1 \pm \left((u_0 + \frac{\eta\sigma\Delta_{SO}}{2})/(E + \frac{\eta\sigma\Delta_{SO}}{2})\right)}$ and $\vec{\tau} = \tau_x\hat{i} + \tau_y\hat{j} + \tau_z\hat{k}$ is the pseudo spin operator with $\hat{k}$ being perpendicular to the graphene plane. For the energy approaching the intrinsic staggered potential $E \to u_o$, we have

$$\langle \vec{\tau} \rangle \cong \hat{k} \tag{17}$$

This one direction of pseudo spin represents the **pseudo-ferrimagnet** defined from the lattice pseudo-spin [75].

Firstly, in Fig. 3, the transport property as a function of the gate potential is investigated, in the case of non-exchange energy h = 0 and non-staggered potential induced energy gap $eE_ZD + u_o = 0$. The spin-valley-dependent energy gap can be described by the formula

$$E_{gap,\eta\sigma} = 2\Delta_{\eta\sigma} = 2\left|\left(\frac{\eta\sigma\Delta_{so}}{2} - \frac{\sigma h}{2} + u_0 + eE_zD\right)\right| \tag{18}$$

and the spin-valley-dependent occupied states are found below

$$E_{F,\eta\sigma} = E + \left(\frac{\eta\sigma\Delta_{so}}{2} + \frac{\sigma h}{2}\right) + \mu \tag{19}$$

For zero exchange energy and staggered potential, plotted in Fig. 3a, the energy gap for all species of electron is $E_{gap,\eta\sigma} = 2\Delta_{so} = 1.3meV$, while the fermi level is different. The occupied states may be found below $E_{F,k\uparrow} = E_{F,k'\downarrow} = E + \frac{\Delta_{so}}{2} + \mu$ and $E_{F,k\downarrow} = E_{F,k'\uparrow} = E - \frac{\Delta_{so}}{2} + \mu$. At $\mu = -6.55meV$, $E_{F,k\downarrow} = E_{F,k'\uparrow} = 0$ centered inside the gap and $E_{F,k\uparrow} = E_{F,k'\downarrow} = 1.3meV$ above the gap (see Fig. 3a). This gate potential value $\mu = -6.55meV$ gives rise to damping state for $k\downarrow$ and $k'\uparrow$, while it is propagating states for $k\uparrow$ and $k'\downarrow$. The general condition to give **damping state,** due to the energy level inside the gap, for electron with spin σ and valley η may be given by

$$-\left(E + \frac{\eta\sigma\Delta_{so}}{2} + \frac{\sigma h}{2}\right) - \frac{E_{g,\eta\sigma}}{2} < \mu < -\left(E + \frac{\eta\sigma\Delta_{so}}{2} + \frac{\sigma h}{2}\right) + \frac{E_{g,\eta\sigma}}{2} \tag{20}$$

For the plotted parameters in Fig. 3, using Eq. (20) we may find the damping state for $k\downarrow$ and $k'\uparrow$ satisfying the condition $-7.2meV < \mu < -5.9meV$. For $k\uparrow$ and $k'\downarrow$, the damping state occurs when $-8.5meV < \mu < -7.2meV$. By this condition, the plot of spin-valley conductance in Fig. 3b shows that $G_{k\uparrow}, G_{k'\downarrow}$ have the same curves and are strongly suppressed due to damping states when $-8.5meV < \mu < -7.2meV$,while $G_{k\downarrow}, G_{k'\uparrow}$ have the same curves and are large, due to propagating states. When $-7.2meV < \mu < -5.9meV$,$G_{k\uparrow}, G_{k'\downarrow}$ exhibit conducting state while $G_{k\downarrow}$, $G_{k'\uparrow}$ are strongly suppressed. This leads to spin-valley-coupled polarization controlled almost completely by the gate (see Fig. 3c). Almost −100% dramatically changes to almost + 100% by varying small gate potential around 7.2 meV. This behavior may be good property for application of gate-control of spin-valley-coupled current with high sensitivity. In non-magnetic barrier, the selectable control of two groups of electron species, "$k\uparrow, k'\downarrow$" and "$k\downarrow, k'\uparrow$", is due to the Fermi level and gap of these two-electron species can be controlled by gate voltage. This result has not been predicted in the previous investigation in other materials [63,65]. The model may be achieved in laboratory, since a non-magnetic-gated-barrier BG/WSe_2-based FET has been recently fabricated [36].

In Fig. 4, the exchange field has been considered. The exchange energy is set to equal to SOI, $h = \Delta_{so} = 1.3meV$, while $eE_ZD + u_o = 0$. In this case, the energy gap of electron of states $k\uparrow$ and $k\downarrow$ is zero. In contrast, the energy gap of electron of states $k'\uparrow$ and $k'\downarrow$ is 2.6 meV. The energy gap and the occupied states are plotted at $\mu = -7.2meV$, to show that for this gate potential electron with states $k\uparrow$ and $k\downarrow$ are allowed to flow through the junction, while electron of states $k'\uparrow$ and $k'\downarrow$ are under damping states and hardly to flow through the junction. In Fig. 4b, it is found that $G_{k\uparrow}$ and $G_{k\downarrow}$ are suppressed only at $\mu = -8.5meV$ and $\mu = -5.9meV$, respectively. This is due to the spin-valley dependent neutron points, touching point between the valence and conduction bands, calculated from $\mu = -\left(E + \frac{\eta\sigma\Delta_{so}}{2} + \frac{\sigma h}{2}\right)$ for the gapless case. For $-8.5meV < \mu < -5.9meV$, $G_{k'\uparrow}, G_{k'\downarrow}$ are almost completely suppressed due to it is under damping states, described by Eq. (20). However, in these gate-potential values, $G_{k\uparrow}$ and $G_{k\downarrow}$ are not suppressed. This behavior leads to the pure valley current (100% of k-valley electron, 100%VP) predicted in Fig. 4c for $-8.5meV < \mu < -5.9meV$. In the case

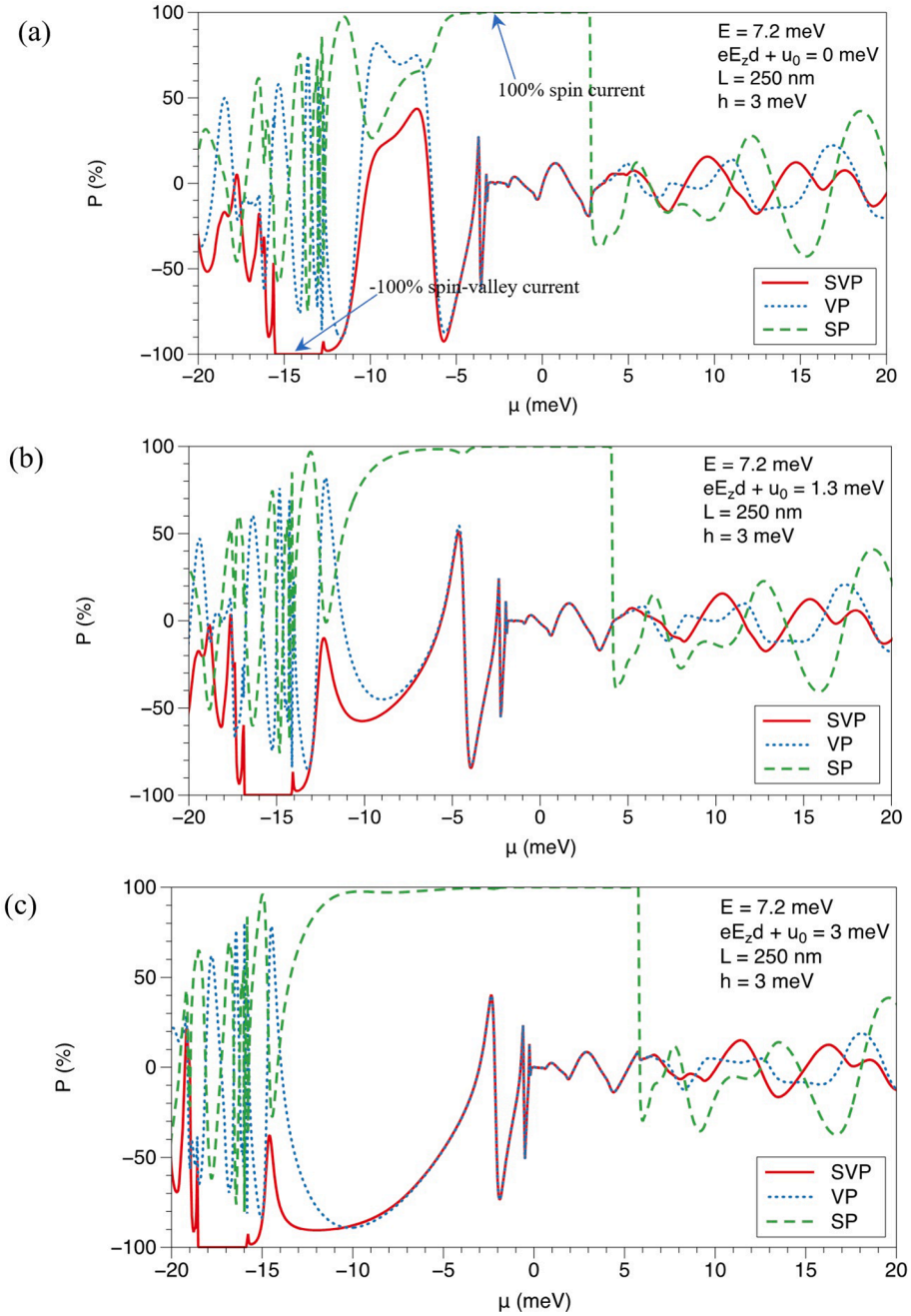

Fig. 7. Study of SVP, VP and SP in the case of $h = 3meV \neq \Delta_{so}$ for $u_0 + eE_zD = 0$, (a) $u_0 + eE_zD = 1.3meV$ (b)and $u_0 + eE_zD = 3meV$(c). The 100% of VP does not appear in this case, while 100% of SVP and SP still appears. Exchange energy of 3 meV may be achieved by depositing $Cr_2Si_2Te_6$ on the top of BG [54].

of non-electric field applied into gated barrier, electron is split into two-valley completely, one valley is suppressed strongly due to its energy level inside the gap, while another valley lies outside the gap, leading to pure valley current for specific gate potential. The current from source to drain may be purely governed by valley current with gate control. This result is to show the junction applicable for valley-based-FET device [60,61,66]. The weak exchange energy induced by depositing magnetic materials on top of gate barrier with $h \simeq \Delta_{so}$ may be achievable using Eu [55,59].

In Fig. 5, the interplay between exchange energy and staggered-potential-induced gap are investigated for $h = eE_ZD + u_o = \Delta_{so} = 1.3meV$. The energy gap from Eq. (19) for $k\uparrow$,$k\downarrow$,$k'\uparrow$ and $k'\downarrow$ are $2.6meV$, $2.6meV$,0 and $5.2meV$, respectively (as seen in Fig. 5a). The Fermi level depends on the gate potential and spin-valley-dependent. By using Eq. (20), the results of $G_{k\uparrow}$ and $G_{k\downarrow}$ are suppressed for $-9.8meV < \mu < -7.2meV$ and $-7.2meV < \mu < -4.6meV$, respectively. Also $G_{k'\uparrow}$ and $G_{k'\downarrow}$ are suppressed at $\mu = -7.2meV$ and $-9.8meV < \mu < -4.6meV$, respectively. In this case, the junction is full spin-valley dependent energy gap and Fermi level. Interestingly, this leads to 100%SP, pure spin current, for $-7.2meV < \mu < -4.6meV$, because only $G_{k\uparrow}$ and $G_{k'\uparrow}$ are not suppressed in this region. Also, 100% SVP, pure spin-valley-coupled current, is predicted for $-9.8meV < \mu < -7.2meV$, because only $G_{k\downarrow}$ and $G_{k'\uparrow}$ are not suppressed in this region. In this case, the junction exhibits both spin and spin-valley FET characteristics. The required condition to give such characteristics is $h = eE_ZD + u_o = \Delta_{so}$. The electric field inside the gate barrier may be easily tuned [2,49].

In Fig. 6, we study switching of spin-valley-coupled current for the

parameters given the same as Fig. 3. The switching of SVP can be controlled perfectly from −100% to + 100% by varying gate potential, when increasing the thickness of the junction large enough L = 400 nm. Suppression of some species of electron requires the decaying length $L >> \xi$ inside the barrier due to decaying state $\psi \sim e^{-x\frac{\sqrt{m\Delta_{so}}}{\hbar}}$, where in this case it may be astimated as $\xi \sim \hbar/\sqrt{m\Delta_{so}} \cong 33nm$. Finally, we study the polarizations in Fig. 7a-7c. The polarizations in the case of $h = 3meV \neq \Delta_{so}$, which may be achieved by depositing $Cr_2Si_2Te_6$ on the top of BG [54]. It is found that the 100% of SP and SVP are controlled able by the gate potential. The two characteristics of spin- and spin-valley FETs devices appeared in this model may show great potential of bilayer graphene doped by WSe_2 and may be achievable.

6. Summary and conclusion

We have investigated spin-valley transport property of bilayer graphene on WSe_2 junction, where the barrier thickness is L. In the barrier, there are layer-dependent proximity-induced exchange field and an applying electric field. The spin-valley dependent transport properties as a function the gate potential in the barrier has been studied. Layer-dependent ferromagnetic bilayer graphene on WSe_2 leads to spin-valley-dependent Fermi energy and energy gap. This has been considered as novel effect of the specific property of BG on WSe_2 system. The transport property due to the effect of interplay between gap and the Fermi energy with depending on spin-valley has been focused. For the excitation energy comparable to SOI, the alignment of pseudo-spin of electron has been found to be only in the z-direction, like a pseudo-ferromagnet. We have found that perfect control of spin-valley-coupled polarization (SVP) from −100% to + 100% by the gate has been predicted, even non-magnetic junction. This junction may be realizable in laboratory [36]. The pure-valley current, 100% of the VP, in the specific values of the gate potential has been predicted, when applying the exchange energy comparable to the SOI strength. The weak exchange energy comparable to SOI strength may be realized by using Eu [55,59]. Also, the pure spin (100% of the SP) and spin-valley-coupled currents have been predicted to occurs when varying different values of the gate potential. In this case, the exchange energy with 3 meV may be generated in the junction by depositing $Cr_2Si_2Te_6$ on the top of BG [54]. This is to say that BG/WSe_2 -based electronics may exhibit multi properties in one system. Our investigation has revealed the potential of BG on WSe_2 for spin-valley-based electronics such as spin-FETs, valley FETs and spin-valley-FETs.

CRediT authorship contribution statement

Kitakorn Jatiyanon: Formal analysis, Software, Investigation, Writing – original draft, Writing – review & editing. **Bumned Soodchomshom:** Supervision, Conceptualization, Methodology, Investigation, Writing – original draft, Writing – review & editing.

Declaration of Competing Interest

The authors declare that they have no known competing financial interests or personal relationships that could have appeared to influence the work reported in this paper.

Data availability

No data was used for the research described in the article.

Acknowledgement

This project is funded by National Research Council of Thailand (NRCT): NRCT5-RSA63002-15.

References

[1] K.S. Novoselov, et al., Science 306 (2004) 666.
[2] A.H.C. Neto, et al., Rev. Mod. Phys. 81 (2009) 109.
[3] M.S. Nevius, et al., Phys. Rev. Lett. 115 (2015), 136802.
[4] S.Y. Zhou, et al., Nat. Mater. 6 (2007) 770.
[5] J. Jung, et al., Nat. Commun. 6 (2015) 6308.
[6] P. Wei, et al., Nat. Mater. 15 (2016) 711.
[7] J.C. Leutenantsmeyer, et al., 2D Materials 4 (2017) 014001.
[8] J. Xu, et al., Nat. Commun. 9 (2018) 2869.
[9] B. Karpiak, et al., 2D Materials 7 (2020) 015026.
[10] C. Tang, et al., Adv. Mater. 32 (2020) 1908498.
[11] H.X. Yang, et al., Phys. Rev. Lett. 110 (2013), 046603.
[12] D.V. Averyanov, et al., ACS Appl. Mater. Interfaces 10 (2018) 20767.
[13] T.K. Chau, et al., npj Quantum Mater. 7 (2022) 27.
[14] A. Hallal, et al., 2D Mater. 4(2017) 025074.
[15] Z. Wang, et al., Phys. Rev. Lett. 114 (2015), 016603.
[16] Y.-F. Wu, et al., Phys. Rev. B 95 (2017), 195426.
[17] Z. Qiao, et al., Phys. Rev. Lett. 112 (2014), 116404.
[18] C. W. J. Beenakker Rev. Mod. Phys. 80(2008)1337.
[19] L. Bretheau, et al., Nat. Phys. 13 (2017) 756.
[20] D.K. Efetov, et al., Nat. Phys. 12 (2016) 328.
[21] B. Soodchomshom, et al., Phys. Lett. A 373 (2009) 3477.
[22] T. Yokoyama Phys. Rev. B 77(2008) 073413.
[23] B. Soodchomshom, et al., Phys. E. 41 (2009) 1475.
[24] C. Si, et al., Nanoscale 8 (2016) 3207.
[25] B. Soodchomshom, P. Chantngarm, J. Supercond. Nov. Magn. 24 (2011) 1885.
[26] T. Fujita, et al., Appl. Phys. Lett. 97 (2010), 043508.
[27] A. Avsar, et al., Nat. Commun. 5 (2014) 4875.
[28] Z. Wang, et al., Nat. Commun. 2015 (2015) 8339.
[29] Z. Wang, et al., Phys. Rev. X 6 (2016), 041020.
[30] B. Yang et al.,2D Materials 3 (2016) 031012.
[31] M. Gmitra, J. Fabian, Phys. Rev. B 92 (2015), 155403.
[32] Z. Gao, et al., J. Phys. Mater. 3 (2020), 042003.
[33] M. Gmitra, J. Fabian, Phys. Rev. Lett. 119 (2017), 146401.
[34] K. Zollner and J. Fabian Phys. Rev. B 104(2021) 075126.
[35] J.O. Island, et al., Nature 571 (2019) 85.
[36] J. Amann, et al., Phys. Rev. B 105 (2022), 115425.
[37] M. Mannaï, S. Haddad, Phys. Rev. B 103 (2021) L201112.
[38] B. Fülöp et al., npj 2D Materials and Applications 5 (2021)82.
[39] C. L. Kane and E. J. Mele Phys. Rev. Lett. 95(2005) 226801.
[40] P. Högl, et al., Phys. Rev. Lett. 124 (2020), 136403.
[41] J. Liu, et al., Phys. Rev. X 9 (2019), 031021.
[42] W.-K. Tse, et al., Phys. Rev. B 83 (2011), 155447.
[43] C.K. Safeer, et al., Nano Lett. 19 (2019) 1074.
[44] M. Gmitra, et al., Phys. Rev. B 93 (2016), 155104.
[45] H. Henck, et al., Phys. Rev. B 97 (2018), 155421.
[46] A.L.R. Manesco, et al., Phys. Rev. B 100 (2019), 125411.
[47] P. Tiwari et al., npj 2D Mater. Appl. 6 (2022) 68.
[48] P. Nualpijit, B. Soodchomshom, Micro Nanostruct. 171 (2022), 207430.
[49] E. McCann, M. Koshino, Rep. Prog. Phys. 76 (2013), 056503.
[50] Y. Cao, et al., Nature 556 (2018) 43.
[51] A. Avsar, et al., ACS Nano 11 (2017) 11678.
[52] J.H. Garcia, et al., Chem. Soc. Rev. 47 (2018) 3359.
[53] G.Hu and B. Xiang Nanoscale Res. Lett. 15 (2020) 226.
[54] K. Zollner, et al., New J. Phys. 20 (2018), 073007.
[55] I.S. Sokolov, et al., Mater. Horiz. 7 (2020) 1372.
[56] X. Zhai, et al., Phys. Rev. Appl. 16 (2021), 014032.
[57] C. Cardoso, et al., Phys. Rev. Lett. 121 (2018), 067701.
[58] T.S. Ghiasi, et al., Nat. Nanotechnol. 16 (2021) 788.
[59] X. Zhai, Y.M. Blanter, Phys. Rev. B 106 (2022), 075425.
[60] M.-K. Lee, et al., Phys. Rev. B 86 (2012), 165411.
[61] R. Li, et al., Phys. Rev. Applied 19 (2023), 024075.
[62] M. Ezawa, Phys. Rev. B 87 (2013), 155415.
[63] B. Soodchomshom, J. Appl. Phys. 115 (2014), 023706.
[64] X. Zhai, et al., Phys. Rev. B 97 (2018), 085410.
[65] H. Li, et al., ACS Appl. Mater. Interfaces 6 (2014) 1759.
[66] R. Liu, et al., Nano Energy 72 (2020), 104678.
[67] A. Srivastava, et al., Nature Phys. 11 (2015) 141.
[68] L.L. Tao, E.Y. Tsymbal, Phys. Rev. B 100 (2019) 161110(R).
[69] C.-C. Liu, H. Jiang, Y. Yao, Phys. Rev. B 84 (2011), 195430.
[70] M. Ezawa Phys. Rev. Lett. 109 (2012) 055502.
[71] P. Chantngarm, K. Yamada, B. Soodchomshom, J. Magn. Magn. Mater 429 (2017) 16.
[72] K. Jatiyanon, B. Soodchomshom, Superlattice. Microst. 120 (2018) 540.
[73] X. Zhai, Phys. Rev. B 105 (2022), 205429.
[74] R. Landauer, IBM J. Res. Dev. 1 (1957) 223.
[75] P. San-Jose, et al., Phys. Rev. Lett. 102 (2009), 247204.